

One-Dimensional Model for Propagation of a Pressure Wave in a Model of the Human Arterial Network: Comparison of Theoretical and Experimental Results

Masashi Saito

Yuki Ikenaga

Mami Matsukawa¹

e-mail: mmatsuka@mail.doshisha.ac.jp

Yoshiaki Watanabe

Laboratory of Ultrasonic Electronics,
Doshisha University,
1-3 Tatara-Miyakodani,
Kyotanabeshi, Kyoto, 610-0321, Japan

Takaaki Asada

Murata Manufacturing Co., Ltd.
10-1, Higashi Kotari 1-chome,
Nagaokakyoshi,
Kyoto 617-8555, Japan
e-mail: asada@murata.co.jp

Pierre-Yves Lagrée

CNRS and Université Pierre et
Marie Curie Paris 06,
Institut Jean le Rond d'Alembert,
Boîte 162, 4 place Jussieu,
75252 Paris, France
e-mail: pierre-yves.lagree@upmc.fr

Pulse wave evaluation is an effective method for arteriosclerosis screening. In a previous study, we verified that pulse waveforms change markedly due to arterial stiffness. However, a pulse wave consists of two components, the incident wave and multireflected waves. Clarification of the complicated propagation of these waves is necessary to gain an understanding of the nature of pulse waves in vivo. In this study, we built a one-dimensional theoretical model of a pressure wave propagating in a flexible tube. To evaluate the applicability of the model, we compared theoretical estimations with measured data obtained from basic tube models and a simple arterial model. We constructed different viscoelastic tube set-ups: two straight tubes; one tube connected to two tubes of different elasticity; a single bifurcation tube; and a simple arterial network with four bifurcations. Soft polyurethane tubes were used and the configuration was based on a realistic human arterial network. The tensile modulus of the material was similar to the elasticity of arteries. A pulsatile flow with ejection time 0.3 s was applied using a controlled pump. Inner pressure waves and flow velocity were then measured using a pressure sensor and an ultrasonic diagnostic system. We formulated a 1D model derived from the Navier-Stokes equations and a continuity equation to characterize pressure propagation in flexible tubes. The theoretical model includes nonlinearity and attenuation terms due to the tube wall, and flow viscosity derived from a steady Hagen-Poiseuille profile. Under the same configuration as for experiments, the governing equations were computed using the MacCormack scheme. The theoretical pressure waves for each case showed a good fit to the experimental waves. The square sum of residuals (difference between theoretical and experimental wave-forms) for each case was <10.0%. A possible explanation for the increase in the square sum of residuals is the approximation error for flow viscosity. However, the comparatively small values prove the validity of the approach and indicate the usefulness of the model for understanding pressure propagation in the human arterial network. [DOI: 10.1115/1.4005472]

Keywords: 1D modeling, wave propagation, human arterial network

1 Introduction

Arteriosclerosis is a vascular condition that leads to cardiovascular disease and stroke. The early stage of arteriosclerosis involves a large increase in aortic stiffness. Atheromatosis then occurs in large and medium-sized arteries with an increase in vessel wall stiffness. This causes arterial stenosis and a reduction in blood flow to the organs, which results in the development of various disorders. Therefore, early diagnosis of the degree of arteriosclerosis is important for reducing the incidence of the disease [1–3].

In recent years, analysis of the pulse wave caused by intravascular pressure has attracted attention as a novel means of diagnosing arterial stiffness. The profile of the pressure wave changes due to wave dispersion [4], and Murgo et al. reported that the profile also clearly changes with increasing arterial stiffness. They also suggested that the intravascular pressure wave is composed of

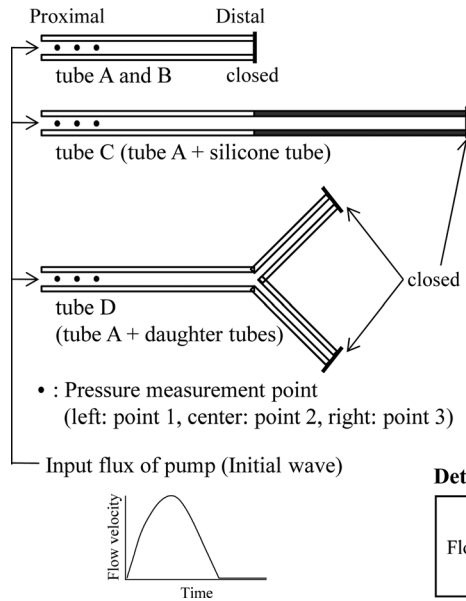
forward and backward pressure waves. The forward pressure wave is caused by blood flow resulting from heart constriction. The backward pressure wave is generated by reflection of the blood flow at peripheral arteries. Because attenuation of the intravascular pressure wave is highly dependent on arterial stiffness, variation in the total intravascular pressure wave is caused by the backward pressure wave [5–7].

In previous studies, we proposed a mathematical technique to separate the backward pressure wave component from the pulse wave for evaluation of arterial stiffness. The maximum amplitude of the backward wave components increases with age, which is consistent with the increase in arterial stiffness due to age [3]. However, it has not yet been clarified where the estimated reflected wave is generated and in which arteries the reflected wave propagates. Clarification of the complicated propagation of these waves is important for an understanding of the nature of pulse waves in vivo.

Numerical computations for biomechanical models have attracted increasing interest because pressure observations at points in arteries by in vitro measurement are nearly impossible. Many researchers have attempted to simulate flow dynamics in

¹Corresponding author.

Contributed by the Bioengineering Division of ASME for publication in the JOURNAL OF BIOMECHANICAL ENGINEERING. Manuscript received July 11, 2011; final manuscript received November 16, 2011; published online December 23, 2011. Assoc. Editor: Rudolph Gleason.



Details of tubes

Tube	Material	Length [mm]	Diameter [mm]	Elasticity [kPa]
A	Polyurethane	2215	8	185
B	Polyurethane	2215	8	85
C	Polyurethane	2215	8	185
	Silicone	30×10^3	8	25×10^3
D	Polyurethane (Mother)	2215	8	185
	Polyurethane (Daughter)	1165	6	185

Details of flow

Flow	Profile	Time interval	Liquid	Total flow volume
	Half cycle of sinusoidal wave	0.3 s	Water	4.5 ml

Fig. 1 Diagram and details of the viscoelastic tubes and the flow input. The pulse flow was input from the left and pressure waves were measured at points 1, 2, and 3. The distance between the input point and the measurement points was 27.5 cm (point 1), 55.0 cm (point 2), and 83.0 cm (point 3).

short straight or bifurcated arteries for a better understanding of circulation system and the effect of arteriosclerosis using 2D axisymmetric or 3D formulations [8–12]. However, these simulations take a long time, so that simulation in a systemic artery is still difficult. A 1D model is an interesting alternative for systemic simulations to avoid complex and time-consuming computations, and can quickly calculate dynamics in a systemic artery and in veins [13–18]. It is well known that the accuracy of 1D modeling is inferior to that of 2D and 3D models owing to the many assumptions used to simplify the governing equations. However, only a few studies have quantitatively evaluated the adequacy of 1D modeling. Moreover, few studies have compared theoretical and experimental results, especially in terms of the simulation accuracy of 1D modeling.

In this study, we evaluated the applicability of a 1D model for pressure wave propagation in flexible tubes. To investigate the validity of the theoretical model, we compared theoretical estimations with measured data obtained from basic models and an artificial arterial network made of soft polymer tubes. The remainder of the paper is organized as follows. In Sec. 2, we describe the basic experiments. Section 3 presents a mechanical model of flow-tube interactions from a 1D point of view. In Sec. 4, the model accuracy and limitations are discussed based on a comparison of numerical and experimental results. Section 5 describes construction of a simple humanlike arterial network with four bifurcations and pressure wave and flow propagation observations in the network. Finally, the experimental results are compared to the theoretical ones.

2 Experiments

2.1 Samples. Four viscoelastic tubes were constructed for basic measurements, as shown in Fig. 1. Two straight tubes (A and B) with a length of 221.5 cm, inner diameter of 8.0 mm, and wall thickness of 2.0 mm were prepared from polyurethane gel (Exseal, Asker-C 5 and 15). The Young's modulus of the polyurethane for tube A was approximately 185 kPa according to a tensile test (Shimadzu, Ez-test), while that for tube B was 85 kPa. The Young's modulus of an aged aorta ranges from 60 to 140 kPa [1]. A silicone tube with a length of 30 m and Young's modulus of approximately 2.5 MPa was connected to the end of tube A to

allow changes in the boundary conditions. For the connection, a urethane rubber tube with length of 1.0 cm, inner diameter of 8.0 mm, and wall thickness of 1.0 mm was used; this length is much smaller than the wave length of a pulse wave. The combined tube was denoted tube C. Daughter tubes made from the same polyurethane gel were connected to the end of tube A. The length, diameter, and thickness of the daughter tubes were 116.5 cm, 6.0 mm, and 2.0 mm, respectively. This bifurcation tube was denoted tube D.

2.2 Experimental Setup. The experimental setup is shown in Fig. 1 and was constructed using a viscoelastic tube and a piston pump (Tomita Engineering, custom-made). The tube was filled with water, and its end was occluded using an acrylic rod to prevent water leakage. A pulse flow with the profile of half a cycle of a sinusoidal wave was input from the pump. The period was 0.3 s and the total flow volume was 4.5 ml. Then pressure waves propagating in the viscoelastic tubes were experimentally measured at three points using a pressure sensor (Keyence, AP-10S). The distance between the input and measurement points was 27.5 cm (point 1), 55.0 cm (point 2), and 83.0 cm (point 3).

2.3 Results. Figure 2 shows pressure waves as a function of time measured at three different points in Fig. 2(a) tube A with elasticity of 185 kPa and Fig. 2(b) tube B with elasticity of 85 kPa. The incident wave, which propagates from the proximal to the distal end, was first observed at the measurement points. The reflected wave was generated at the distal end and propagated back to the proximal end. Then propagation and reflection of the pressure wave repeated at the proximal and distal ends, which resulted in the observation of multiple reflected waves. There was a marked difference in the number of reflected waves between tubes A and B. This can be explained by the difference in Young's modulus for the tubes. The velocity seemed to be proportional to the square root of the Young's modulus of the tube material [19].

Figure 2(c) shows the pressure waves in tube C, comprising a long silicone tube connected to tube A. Although the first reflected waves for tubes A [Fig. 2(a)] and C [Fig. 2(c)] occurred at the same time and the number of waves was the same, the amplitude of the reflected wave at point 1 in tube C was 61% of that in tube A. This indicates that partial reflection of the pressure wave

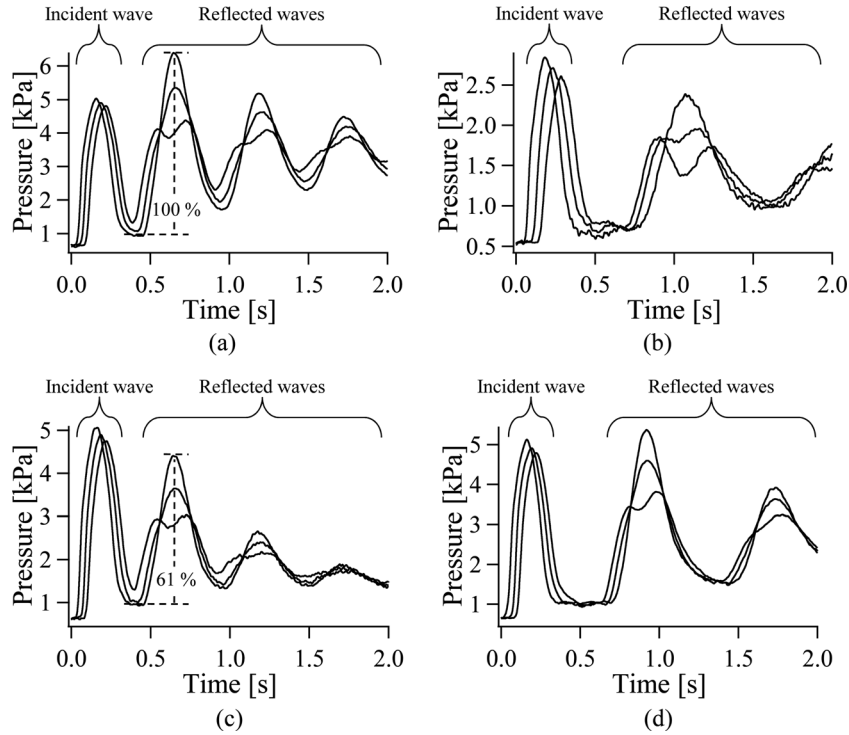


Fig. 2 Time series of pressure waves in viscoelastic tubes measured at three points for tubes (a) A, (b) B, (c) C, and (d) D

occurred at the connection point owing to the difference in tube admittance. Furthermore, considering the length (30.0 m) and wave velocity for the silicone tube, the transmitted pressure wave cannot propagate back and be observed again within the measurement time.

Figure 2(d) shows pressure waves in the bifurcation tube. Considering the arrival time of the first reflected wave in tube A, wave reflection was not caused by the bifurcation point. Thus, the reflected waves observed were generated by reflection at the distal end of the daughter tubes.

3 Basic Equations

3.1 Flow Dynamics in a Flexible Tube. We describe here the formulation of 1D model to simulate theoretical waves in flexible tubes. The equation of continuity and the Navier-Stokes equations in a cylindrical coordinate system are used as the governing equations. Considering 2D axisymmetric flow in a long flexible tube with a small radius, the simplified governing equations for a long wave approximation are given by

$$\frac{1}{r} \frac{\partial}{\partial r} (rv) + \frac{\partial u}{\partial x} = 0 \quad (1)$$

$$\frac{\partial u}{\partial t} + u \frac{\partial u}{\partial x} + v \frac{\partial u}{\partial r} = -\frac{1}{\rho} \frac{\partial P}{\partial x} + \frac{\nu}{r} \frac{\partial}{\partial r} \left(r \frac{\partial u}{\partial r} \right) \quad (2)$$

$$0 = -\frac{1}{\rho} \frac{\partial P}{\partial r} \quad (3)$$

Here, the momentum equation and all derivations in the circumferential direction are omitted because the velocity in the ϕ -direction is zero. We note that the pressure does not change across the section, and transverse viscous effects are negligible.

Formulation of analytical solutions from the equation of continuity and the Navier-Stokes equations is generally impossible. Moreover, numerical solutions with a fluid-structure interaction are complicated and time-consuming. Thus, instead of using a 3D field,

a mean field for the velocity and flux obtained by integration over the cross-section are introduced as a simple numerical technique. After multiplying by $2\pi r$ and integrating both equations over the cross-section, we then derive 1D equations from Eqs. (1) and (2)

$$\frac{\partial A}{\partial t} + \frac{\partial Q}{\partial x} = 0 \quad (4)$$

$$\frac{\partial Q}{\partial t} + \frac{\partial}{\partial x} \left(2\pi \int_0^{R_0} ru^2 dr \right) = -\frac{A}{\rho} \frac{\partial P}{\partial x} + 2\pi\nu \left[r \frac{\partial u}{\partial r} \right]_{r=R_0} \quad (5)$$

where A is the tube cross-section. Q is the flux, defined as

$$Q = \int_0^{R_0} 2\pi r u dr \quad (6)$$

The flow velocity profile as a function of radius changes owing to the Womersley number, defined as $\alpha = R_0 \sqrt{\omega/\nu}$. In general, governing equations should be computed from the velocity profiles with arbitrary α . In this paper, we make assumption for the velocity profile for simplicity. Exact estimation of skin friction is a weak point of integral methods. A common approximation is that the flow profile remains close to a Hagen-Poiseuille profile. However, the flow is actually neither a Poiseuille nor a Womersley profile. To circumvent this problem, several approximations have been developed. For example, Zagzoule and Marc-Vergnes constructed an expansion of Poiseuille friction with unsteady corrections [15], whereas other researchers constructed a complicated closure using an extra equation [13], or proposed an extra complicated profile [20]. Other authors have used a priori estimates [16,21]. In the latter two papers, no reference to the unsteady Womersley solution is considered. In some more mathematical papers, viscosity is sometimes neglected [22]. In the present study, we take the simplest model, bearing in mind that it should be corrected in the future. The effect of the exact profile on the nonlinear term may also be discussed

$$2\pi \int ru^2 dr = \gamma \left(\frac{Q^2}{A} \right) \quad (7)$$

A flat profiles gives $\gamma = 1$, whereas a Poiseuille profile gives $\gamma = 4/3$. As we see in the order of magnitude analysis, this term is small, and changing $\gamma = 4/3$ to $\gamma = 1$ has little influence on the results. Using this simple approximation, the two terms of Eq. (5) become

$$\frac{\partial}{\partial x} \left(2\pi \int_0^{R_0} ru^2 dr \right) = \frac{4}{3} \frac{\partial}{\partial x} \left(\frac{Q^2}{A} \right), \quad 2\pi\nu \left[r \frac{\partial u}{\partial r} \right]_{r=R_0} = \frac{8\nu Q}{R^2} \quad (8)$$

Finally, the governing equations for a Hagen-Poiseuille profile are Eqs. (4) and (5) in which (8) is substituted.

3.2 Nondimensional Governing Equations. We derive nondimensional governing equations to simulate pressure propagation in flexible tubes of different inner diameter, Young's modulus, and thickness. The governing equations are

Conservation of mass

$$\frac{\partial A}{\partial t} + \frac{\partial Q}{\partial x} = 0$$

Momentum equation

$$\frac{\partial Q}{\partial t} + \frac{4}{3} \frac{\partial}{\partial x} \left(\frac{Q^2}{A} \right) = -\frac{A}{\rho} \frac{\partial P}{\partial x} - \frac{8\nu Q}{R^2} \quad (9)$$

We now explain the pressure law. When a pressure wave propagates in a distensible tube, it is progressively attenuated, and its amplitude decreases exponentially during propagation. The attenuation is mainly caused by the viscosity of the walls. Furthermore, the stress-strain relation for flexible tubes such as arteries is nonlinear [1]. Thus, the pressure law is formulated as a single nonlinear term and an attenuation term according to the Kelvin-Voigt model

$$P = K((R - R_0) + \varepsilon_p(R - R_0)^2) + \eta \frac{\partial R}{\partial t} \quad (10)$$

where ε_p is a small nonlinearity parameter. η is proportional to the viscosity of the tube wall and is unknown, so it needs to be estimated from measurement data. The longitudinal tension terms are also ignored [13]. This approximation neglects the second-order derivative term for displacement of the artery as a function of tension. This is consistent with our experiments, but it should be reintroduced in the future as dispersion effects have been observed in humans [4]. We introduce the following dimensional variables and derive nondimensional equations to yield a simple computation

$$t = T_0 \bar{t} \quad x = L_0 \bar{x} = c_0 T_0 \bar{x} \quad Q = Q_0 \bar{Q} \quad h = h_0 \bar{h} \quad E = E_0 \bar{E}$$

$$R = R_0 \bar{R}_{df} + \Delta R \bar{R} \quad A = A_0 \bar{A} = \pi R_0^2 \left(\bar{R}_{df}^2 + 2 \frac{\Delta R}{R_0} \bar{R}_{df} \bar{R} \right)$$

$$K = \frac{E}{1 - \sigma^2} \frac{h}{R^2} = \frac{E_0}{1 - \sigma^2} \frac{h_0}{R_0^2} \frac{\bar{E} \bar{h}}{\bar{R}_{df}^2} = K_0 \bar{K}$$

where constants T_0 , L_0 , Q_0 , h_0 , E_0 , R_0 , ΔR , A_0 , and K_0 are orders of magnitude of the dimensional variables. For the flux, we choose the maximum value. Nondimensional variables \bar{t} , \bar{x} , \bar{Q} , \bar{h} , \bar{E} , \bar{R}_{df} , \bar{R} , \bar{A} , and \bar{K} are of order 1, which means that they fall in the range between 0 and 10.0. \bar{E} , \bar{h} , \bar{K} , and \bar{R}_{df} are functions of the position (note that for a straight homogeneous tube, they are constants of value 1.0). c_0 is the Moens-Korteweg velocity, defined as

$$c_0 = \sqrt{\frac{K_0 R_0}{2\rho}} = \sqrt{\frac{E_0}{1 - \sigma^2} \frac{h_0}{2\rho R_0}} \quad (11)$$

where K_0 is defined as $E_0 h_0 / R_0^2 (1 - \sigma^2)$. The equation gives the velocity of the pulse wave as a function of the tube elasticity. Substituting the variables and the pressure law into the conservation of mass and momentum equations, the leading terms, which are $Q_0 T_0 / 2\pi R_0 \Delta R L_0$ and $A_0 K_0 \Delta R T_0 / \rho L_0 Q_0$, are regarded as unity to obtain the pertinent nondimensional variables. Finally, we obtain the nondimensional governing equations

Conservation of mass

$$\bar{R}_{df} \frac{\partial \bar{R}}{\partial \bar{t}} = -\frac{\partial \bar{Q}}{\partial \bar{x}} \quad (12)$$

Momentum equation

$$\frac{\partial \bar{Q}}{\partial \bar{t}} + \frac{4}{3} \frac{Q_0 T_0}{A_0 L_0} \frac{\partial}{\partial \bar{x}} \left(\frac{\bar{Q}^2}{\bar{R}_{df}^2} \right) = -\bar{R}_{df}^2 \frac{\partial (\bar{K} \bar{R})}{\partial \bar{x}} - \bar{\varepsilon}_p \bar{R}_{df}^2 \frac{\partial (\bar{K} \bar{R}^2)}{\partial \bar{x}} + \bar{\varepsilon}_v \bar{R}_{df} \frac{\partial^2 \bar{Q}}{\partial \bar{x}^2} - \frac{8\nu T_0 \bar{Q}}{R_0^2 \bar{R}_{df}^2} \quad (13)$$

with $\bar{\varepsilon}_p = \varepsilon_p \Delta R$ and $\bar{\varepsilon}_v = \eta / (K_0 T_0)$. Moreover, the leading term is converted to the following using the propagation velocity

$$\frac{\Delta R}{R_0} = \frac{Q_0}{2A_0 c_0} = \varepsilon \quad (14)$$

where ε is equal to the change ratio of tube radius.

3.3 Computation. The differential equations were computed using the MacCormack method [14,23]. The MacCormack scheme is a two-step predictor-corrector technique with three points in space and two levels in time with second-order accuracy for time and space. The governing equation in conservative form is

$$\frac{\partial \mathbf{V}}{\partial t} + \frac{\partial \mathbf{F}}{\partial x} + \mathbf{S} = 0 \quad (15)$$

where $\mathbf{V} = (\bar{R}, \bar{Q})$, is a vector of dynamical variables,

$\mathbf{F} = \left(-\frac{1}{\bar{R}_{df}} \bar{Q}, -\bar{R}_{df}^2 \frac{\partial (\bar{K} \bar{R})}{\partial \bar{x}} - \bar{\varepsilon}_p \bar{R}_{df}^2 \frac{\partial (\bar{K} \bar{R}^2)}{\partial \bar{x}} - \frac{4}{3} \frac{Q_0 T_0}{A_0 L_0} \left(\frac{\bar{Q}^2}{\bar{R}_{df}^2} \right) \right)$ is a vector of conserved quantities, and $\mathbf{S} = \left(0, \bar{\varepsilon}_v \bar{R}_{df} \frac{\partial^2 \bar{Q}}{\partial \bar{x}^2} - \frac{8\nu T_0 \bar{Q}}{R_0^2 \bar{R}_{df}^2} \right)$ is the

source term. The difference equations are finally given by

Predictor step

$$\mathbf{V}_i^* = \mathbf{V}_i^n - \frac{\Delta t}{\Delta x} (\mathbf{F}_{i+1}^n - \mathbf{F}_i^n) - \Delta t \mathbf{S}_i^n \quad (16)$$

Corrector step

$$\mathbf{V}_i^{n+1} = \frac{1}{2} (\mathbf{V}_i^n + \mathbf{V}_i^*) - \frac{\Delta t}{2\Delta x} (\mathbf{F}_i^* - \mathbf{F}_{i-1}^*) - \frac{\Delta t}{2} \mathbf{S}_i^* \quad (17)$$

To construct numerical tube models, details of the experimental tubes were used. The experimentally observed wave at the pump input point was used for the dimensionless input flux and its profile is shown in Fig. 1. To determine the optimum simulation result, we varied three parameters: elasticity $E_0/(1 - \sigma^2)$ (range 40–300 kPa, step size 5 kPa), attenuation $\bar{\varepsilon}_p$ (range 0.010–0.080, step size 0.002), and nonlinearity $\bar{\varepsilon}_p$ (range 0.010–0.080, step size 0.002). To evaluate the quality of the simulated waves, we calculated square sum of differences between the theoretical and experimental waveforms (cost function) at point 1 according to [13]

$$J = \frac{1}{T_m} \int_0^{T_m} (f_s - f_m)^2 dt \quad (18)$$

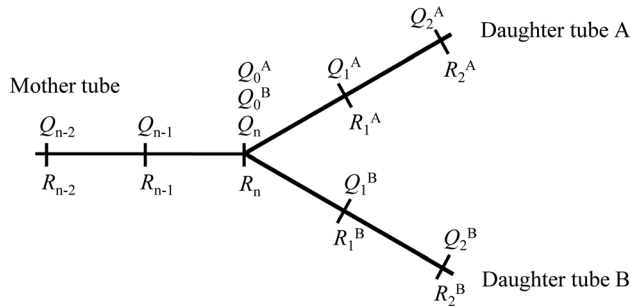


Fig. 3 Discrete values of the radius (R) and flux (Q) in mother and daughter tubes. Superscripts A and B denote daughter tubes A and B. Subscripts denote the position in the tube.

where f_s and f_m are the theoretical and experimental pressure waves at point 1 and T_m is the measurement time. Finally, the wave with the smallest dispersion was adopted. An example of a typical cost function minimization is shown in Fig. 4.

3.4 Boundary Conditions. Setting of the boundary conditions is key in proper simulations. For the boundary conditions at the tube entrance and exit, complete reflection should occur. We set these as follows:

$$Q = 0, \quad \frac{\partial R}{\partial x} = 0$$

We next describe simulation of pressure wave propagation in a bifurcated tube. An important issue is the boundary conditions at the bifurcation. Figure 3 shows discrete values for the radius and flux in the mother and daughter tubes. Superscripts A and B denote daughter tubes A and B, respectively. Subscripts denote positions in the tubes. We calculate the radius at the bifurcation point R_n using the following expression

$$R_n = \frac{1}{3} (R_{n-1} + R_1^A + R_1^B) \quad (19)$$

Here we assume that pressure loss and the effect of the angle of the daughter tube to the mother tube are negligible. We assume that the flux satisfies the conservation of mass expressed as $Q_n = Q_0^A + Q_0^B$ at the bifurcation. Q is the flux propagating in the mother tube, and Q^A and Q^B are those in the daughter tubes. From these assumptions and the conservation of mass, the flux boundary condition is

$$Q_n = \frac{1}{3} (2Q_{n-1} + Q_1^A + Q_1^B), \quad Q_0^A = \frac{1}{3} (Q_{n-1} + 2Q_1^A - Q_1^B), \\ Q_0^B = \frac{1}{3} (Q_{n-1} - Q_1^A + 2Q_1^B) \quad (20)$$

4 Comparison of Experimental and Theoretical Estimates

To simulate the best-matching theoretical waves, the cost functions described by Eq. (18) were used. Figure 4 shows an example of the cost function, with the optimum parameters estimated as $E_0/(1 - \sigma^2) = 250$ kPa, $\bar{\epsilon}_v = 0.034$, and $\bar{\epsilon}_p = 0.046$. Figure 5 shows the theoretical pressure waves at each point with the optimum coefficients. The trend for the theoretical wave is in good agreement with that for the experimentally observed wave.

The influence of nonlinearity and attenuation of the tube wall, fluid viscosity and convection effects on the theoretical waves was assessed. Figure 6 compares the wave measured at point 1 and the theoretical wave for four conditions. Comparison of Figs. 6(c) and 6(d) reveals the effect of nonlinearities.

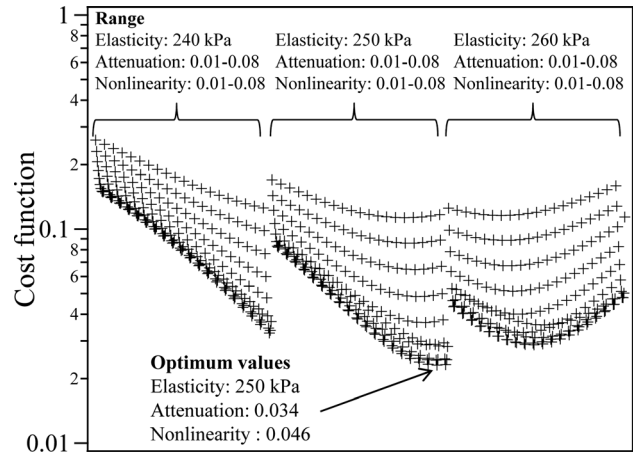


Fig. 4 Example of cost functions calculated from elasticity $E_0/(1 - \sigma^2) = 240, 250,$ and 260 kPa, attenuation $\bar{\epsilon}_v = 0.01 - 0.08$, and nonlinearity $\bar{\epsilon}_p = 0.01 - 0.08$. The optimum parameters for pressure waves in tube A were estimated as $E_0/(1 - \sigma^2) = 250$ kPa, $\bar{\epsilon}_v = 0.034$, and $\bar{\epsilon}_p = 0.046$.

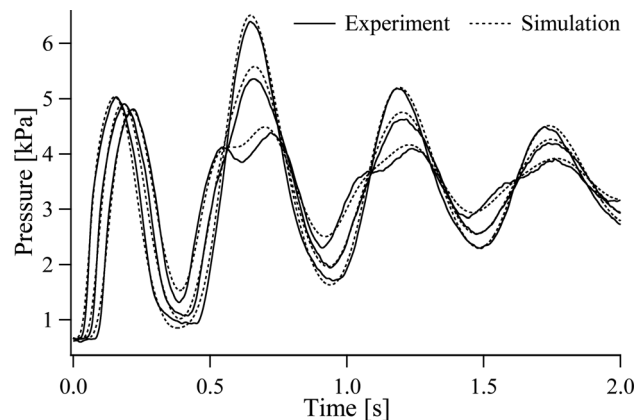


Fig. 5 Experimental and theoretical pressure waves as a function of time (tube A). The optimum parameters used were estimated as $E_0/(1 - \sigma^2) = 250$ kPa, $\bar{\epsilon}_v = 0.034$, and $\bar{\epsilon}_p = 0.046$.

Comparison of Figs. 6(a) and 6(b) indicates that the attenuation seems to be highly underestimated. Furthermore, the pulse width of the theoretical wave in Fig. 6(a) is still short. Therefore, the viscoelasticity of the tube wall should be a dominating factor in the pulse attenuation. Comparison of Figs. 6(b), 6(c), and 6(d) shows a clear difference in the nonlinear effects of convection and the tube wall. The effect of fluid nonlinearity is small in Fig. 6(c) and increases in Fig. 6(d). Thus, nonlinearity of the tube wall is an important factor. Finally, a pressure law including both attenuation and nonlinearity of the tube wall is necessary to accurately simulate waves in a straight flexible tube.

Figure 7 shows pressure waves propagating in tube B. The optimum parameters were $E_0/(1 - \sigma^2) = 75$ kPa, $\bar{\epsilon}_v = 0.070$, and $\bar{\epsilon}_p = 0.070$ according to the cost functions. The theoretical waves were in good agreement with the experimental results. Assuming a Poisson ratio of 0.5 (pure rubber), Young's modulus E_0 calculated from $E_0/(1 - \sigma^2)$ was approximately 188 kPa for tube A and 56 kPa for tube B. Thus, the estimated and experimental values are in good agreement. Therefore, we conclude that our simple 1D model is useful for simulating flow dynamics in straight tubes.

We then simulated waves in tubes of different elasticity (tube C) and in a single bifurcated tube (tube D). Figures 8 and 9 compare the measured and simulated results. We used the same optimum parameters as for tube A ($E_0/(1 - \sigma^2) = 250$ kPa, $\bar{\epsilon}_v = 0.034$,

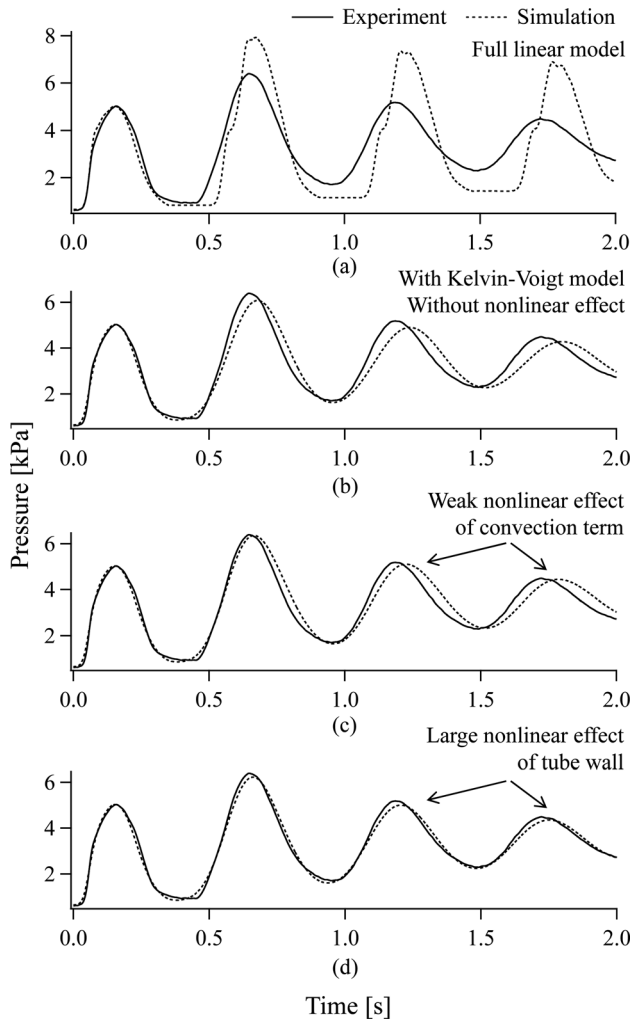


Fig. 6 Comparison of the wave measured at point 1 and theoretical waves calculated for four conditions: (a) $E_0/(1 - \sigma^2) = 250$ kPa, $\bar{\epsilon}_v = 0.0$, $\bar{\epsilon}_p = 0.0$, and no fluid convection effect; (b) $E_0/(1 - \sigma^2) = 250$ kPa, $\bar{\epsilon}_v = 0.034$, $\bar{\epsilon}_p = 0.0$, and no fluid convection effect; (c) $E_0/(1 - \sigma^2) = 250$ kPa, $\bar{\epsilon}_v = 0.034$, $\bar{\epsilon}_p = 0.0$, and a fluid convection effect; and (d) $E_0/(1 - \sigma^2) = 250$ kPa, $\bar{\epsilon}_v = 0.034$, $\bar{\epsilon}_p = 0.046$, and no fluid convection effect.

and $\bar{\epsilon}_p = 0.046$) because tubes A, C, and D were made from the same polymer. Consequently, the simulated pressure waves in tube C were similar to the measured waves. The theoretical reflection coefficient was calculated as approximately 0.57. This phenomenon can be explained by the tube admittance. In general, the reflection coefficient for pressure is defined as $P_r/P_i = (Y_0 - Y_1)/(Y_0 + Y_1)$ with admittance $Y = A/\rho c$ [24], where subscripts i and r denote incident and reflected waves and Y_0 and Y_1 are the admittance of each tube. The only difference was in elasticity between the soft tube (188 kPa) and the silicone tube (2.5 MPa). Thus, the theoretical value was 0.57, which was quite near the experimental value of 0.61. This confirms that the partial reflection at the interface can be estimated properly by the above equations.

The accuracy of the simulated waves for tube D was moderate. The amplitude and down-stroke of the reflected wave have small errors, and the square sum of residuals (difference between the two waveforms) was $< 5.8\%$. In particular, the downstroke of the measured reflected wave showed a gentle slope compared with the theoretical wave. This phenomenon could not be simulated perfectly using the elasticity, attenuation, and nonlinearity parameters. Meanwhile, the offset was easily influenced by the flow viscosity expressed as $8\nu Q/R^2$ in Eq. (9). An increase in flow

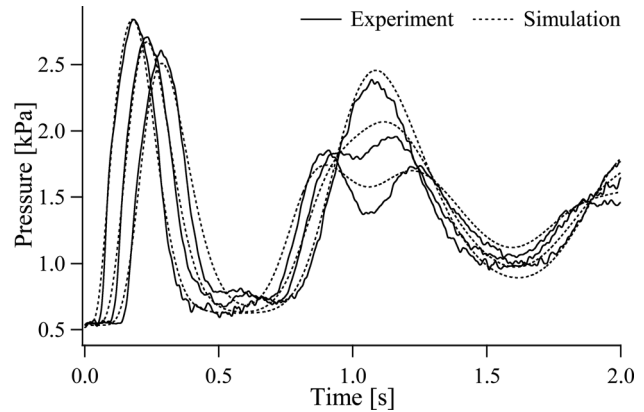


Fig. 7 Experimental and theoretical pressure waves in tube B. The optimum parameters used were estimated as $E_0/(1 - \sigma^2) = 75$ kPa, $\bar{\epsilon}_v = 0.070$, and $\bar{\epsilon}_p = 0.070$.

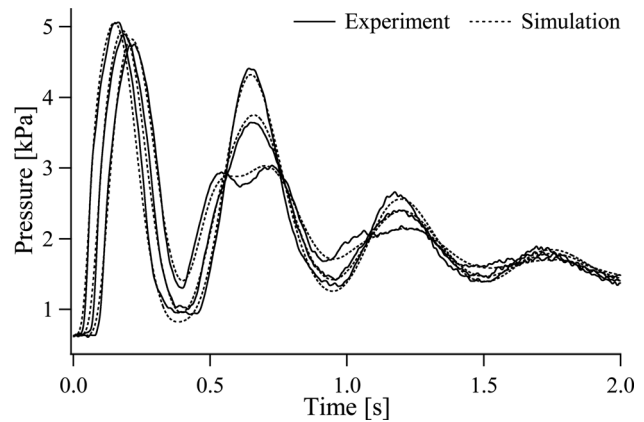


Fig. 8 Experimental and theoretical pressure waves in tube C. The optimum parameters used were estimated as $E_0/(1 - \sigma^2) = 250$ kPa, $\bar{\epsilon}_v = 0.034$, and $\bar{\epsilon}_p = 0.046$.

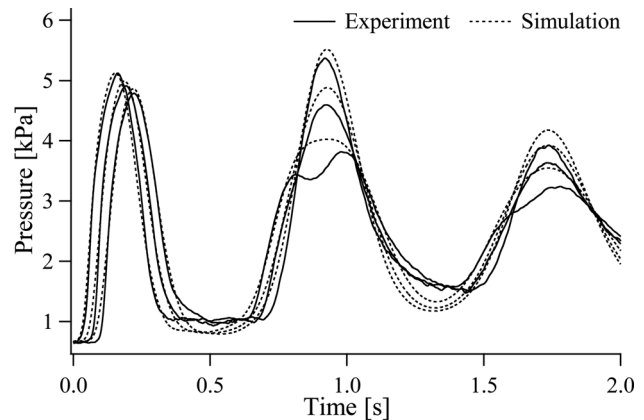


Fig. 9 Experimental and theoretical pressure waves in tube D. The optimum parameters used were estimated as $E_0/(1 - \sigma^2) = 250$ kPa, $\bar{\epsilon}_v = 0.034$, and $\bar{\epsilon}_p = 0.046$.

viscosity using a coefficient of 2.0 or 3.0 led to a marked increase in the offset level, and the amplitude of the reflected waves could not be simulated properly (Fig. 10). This indicates that the main error seems to arise from the flow viscosity. Thus, the common approximation, which is that the steady flow profile remains close to a Hagen-Poiseuille profile, leads to a difference in the offset

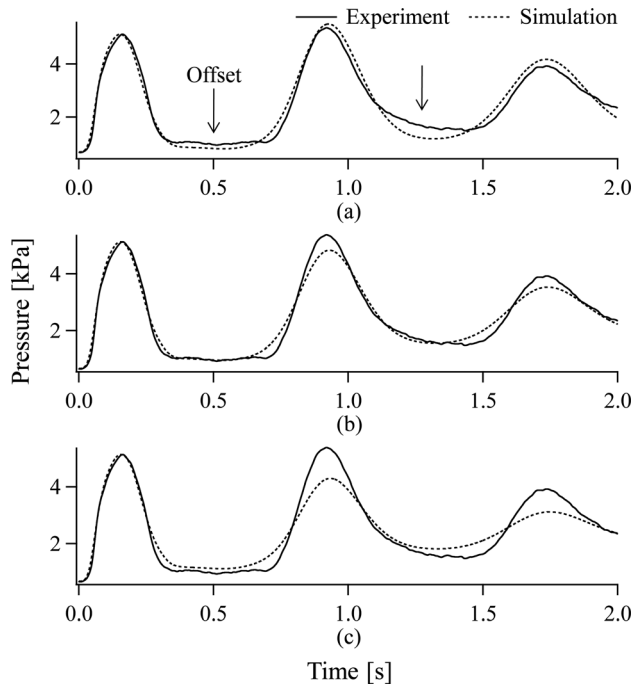


Fig. 10 Effect of fluid viscosity on the pressure wave at point 1. An increase in flow viscosity involving a coefficient of (a) 1.0, (b) 2.0, or (c) 3.0 leads to marked augmentation of the offset level.

level. In the mother tube, the Womersley number calculated from the tube configuration $R_0 = 4.0$ mm, $\nu = 1.0 \times 10^{-6}$ m²/s, and $T_0 = 0.3$ s is $\alpha = 12.94$. Figure 11 compares velocity profiles for a Womersley flow with $\alpha = 12.94$ and a Hagen-Poiseuille flow of the same flux for an oscillating flow input. The flow velocity profiles clearly differ and it is likely that this term yields errors. To improve the simulation accuracy, other closures of the viscous resistance need to be introduced. However, we found many similarities in the waves. For instance, the arrival time and amplitude of both forward and reflected waves, and the reflection condition at the bifurcation point were well simulated. Thus, from the point of view of the simple case, we conclude that our 1D model is applicable for simple analysis of flow dynamics in viscoelastic tubes.

5 Human Artery Model

After validating the model in basic experiments, we constructed experimental and numerical human artery models with four bifurcations and measure and calculated the pressure and average flow velocity. Finally, we evaluated the applicability of the 1D model for a minimal arterial network.

5.1 Model Definition. Figure 12 shows a schematic of our simple human arterial model with four bifurcations. The model was constructed with an aorta and femoral, subclavian, radial, and left carotid arteries in a configuration based on a previous study by Westerhof et al. [25]. Polymer tubes with an elasticity of 185 kPa (Shimadzu, Ez-test) were used for each artery. The elasticity of the aorta obtained from senior subjects is 60–140 kPa [1], so the constructed tubes had higher elasticity than an actual human artery. In a human artery, reflection of the intravascular pressure wave does not occur at each bifurcation. Therefore, the tube diameter and thickness do not induce reflected waves.

Peripheral sites of the model are regarded as reflection points, such as vascular beds or peripheral blood vessels in the human body. It has been reported that reflection coefficients at these points are approximately 0.7–0.8 [1]. To realize these reflection coefficients, silicone tubes were connected as virtual peripheral

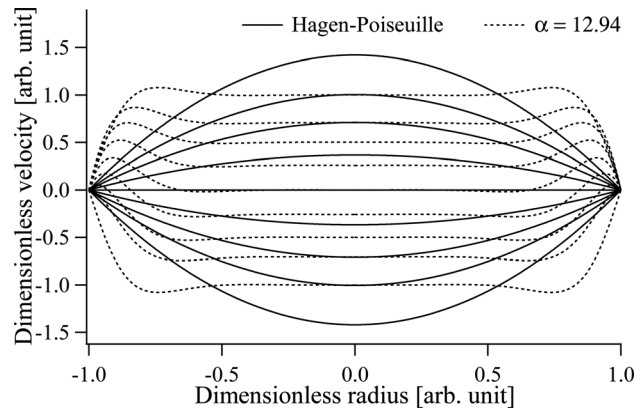


Fig. 11 Comparison of velocity profiles for a Womersley flow with $\alpha = 12.94$ and a Hagen-Poiseuille flow of the same flux

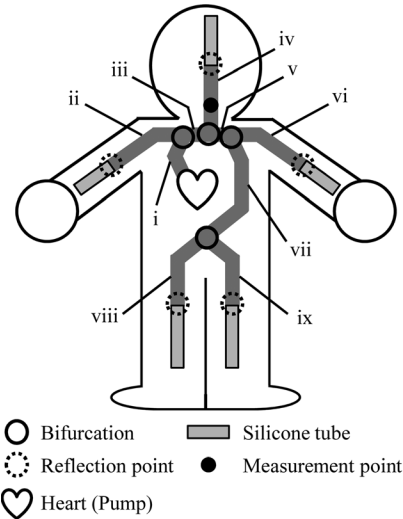
sites at the end of the tubes. The diameter, thickness, and elasticity of the silicone tubes were 8.0 mm, 2.0 mm, and 2.5 MPa, respectively. The elasticity of the silicone tubes was much higher than that of the polyurethane tubes. The actual reflection coefficient at these connection points was determined to be approximately 0.50 in a preliminary experiment.

5.2 Experimental and Simulation Details. In this comparison, we focused on the pressure wave and average flow velocity in the common carotid artery. The pressure wave was measured using the experimental setup described in Sec. 2.2. The average flow velocity was measured using an ultrasonic Doppler system (Toshiba Medical Systems, Aplio SSA-700A). The center frequency of the ultrasonic pulse used (Toshiba Medical Systems, Probe PLT-1204AT) was 12 MHz. The incident angle of the ultrasonic beam was set to approximately 45° from the vertical direction. By performing incident angular correction, we obtained the actual flow velocity waveform. A model of the theoretical artery model was constructed using the same details as for the soft tubes and the experimental setup. Then we calculated the optimum pressure and flow velocity in the common carotid artery using the cost functions.

5.3 Comparison of Experimental and Theoretical Estimates. Figures 13 and 14 compare the experimental and theoretical pressure waves and flow velocities. The coefficients determined from the cost functions were $E_0/(1 - \sigma^2) = 170$ kPa, $\bar{e}_p = 0.036$, and $\bar{e}_p = 0.010$. The theoretical waves are in good agreement with the experimental waves. Considering the complicated profiles of the experimental and theoretical waves, they probably consist of many waves reflected from peripheral parts. Moreover, the experimental pressure waveform was similar to the pulse wave in vivo [1].

The trend for the theoretical pressure wave shows a close fit to that for the measured wave.

Although the square sum of residuals for the pressure wave is slightly greater, the values were all <10.0% of the maximum amplitude. One possible explanation for the underestimated pressure attenuation is an approximation error for the fluid viscosity. The amplitude of the estimated velocity is slightly smaller than the amplitude of the measured wave. The difference could be due to measurement errors. For example, there is a possibility that the measured flow velocity was underestimated because of scattering of the ultrasonic beam. However, the trends for the two waves are quite similar. Therefore, the comparatively small differences between the theoretical and experimental waves prove the validity of this approach and indicate that it is useful in furthering our understanding of the dynamics of flow propagation in a real human artery.



	Name	Length [mm]	Diameter [mm]	Thickness [mm]
i	Aorta arch A	35	12	2
ii	R.subclavian radial artery	800	6	1.5
iii	Aorta arch B	20	11	2
iv	L.carotid artery	675	6	1.5
v	Aorta arch C	40	10	2
vi	L.Subclavian radial artery	710	6	1.5
vii	Aorta	470	8	1.5
viii	R.femoral artery	365	6	1.5
ix	L.femoral artery	365	6	1.5

Fig. 12 Structure of the simple arterial network and part details. Silicone tubes were connected to the flexible tubes to model reflection points. The measurement position was at the left carotid artery.

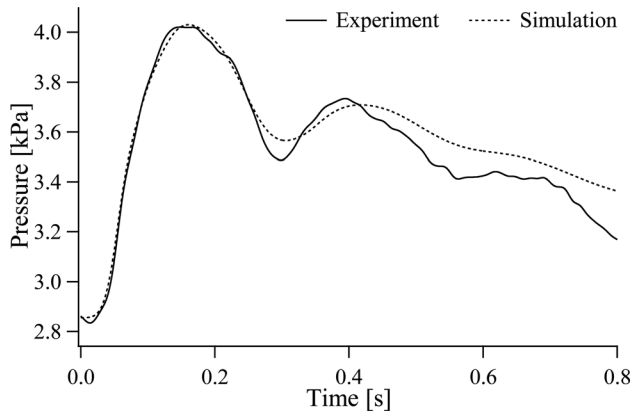


Fig. 13 Time series of measured and simulated pressure waves in the simple human artery model. The optimum parameters used were estimated as $E_0/(1 - \sigma^2) = 170$ kPa, $\bar{\varepsilon}_v = 0.036$, and $\bar{\varepsilon}_p = 0.010$.

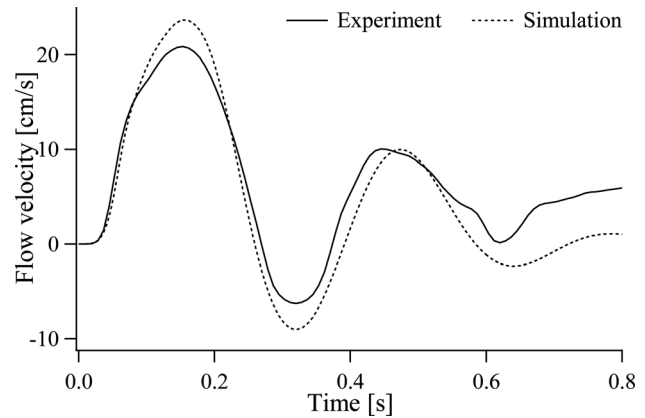


Fig. 14 Time series of measured and simulated flow velocity waves in the simple human artery model. The optimum parameters used were estimated as $E_0/(1 - \sigma^2) = 170$ kPa, $\bar{\varepsilon}_v = 0.036$, and $\bar{\varepsilon}_p = 0.010$.

6 Conclusion and Perspectives

A 1D model to simulate pressure perturbations in flexible tubes was described, and its applicability was validated by comparison with the experimental results. Pressure waves propagating in different viscoelastic tubes were experimentally measured. Under the same experimental conditions, the pressure waves were then calculated by the numerical model. Consequently, the following facts were clarified from the comparisons of experimental and theoretical results:

- (1) The theoretical results fit well with the experimental results, and tube elasticity estimates obtained from the minimum cost function were similar to the values obtained from tensile tests.
- (2) The effects of attenuation and nonlinearity of the tube wall were greater than those of fluid viscosity and convection.
- (3) There is a possibility that the proposed 1D model includes a small error for viscosity, which was derived from the Hagen-Poiseuille profile, so other models should be tested.

Measured and simulated pressure waves and flow velocities in the human artery model were compared. Even though the propagation pattern was quite complicated, the results fit well with the experimental results. This indicates that the experimental and numerical models are suitable for human applications. Thus, we can

conclude that our model is acceptable and will be useful in gaining an understanding of the flow dynamics in flexible tubes and in human arteries.

We have recently started a further investigation into models with more bifurcations and the effects of other approximation terms for viscosity. In addition, tapered tubes and tubes with dilatations or constrictions should be explored. Moreover, terminal reflection such as in the Windkessel model should be introduced into experimental set-ups. After these investigations, the reliable 1D model is strongly expected to simulate flow dynamics in systemic arterial tree of healthy subjects. Furthermore, if we add some locally more refined models, we could be able to observe the influence of stenosis [26] or aneurysms. Such models of the arterial tree are necessary to set good boundary conditions for a full Navier-Stokes solution for elastic walls in a multiscale approach [27,28].

Nomenclature

- u = longitudinal wave velocity
- h = thickness of the viscoelastic tube
- h_0 = unperturbed thickness of the viscoelastic tube
- P = pressure
- P_0 = initial pressure
- x = longitudinal variable

r = radial transversal variable
 t = time
 T_0 = time scale
 R = tube radius
 R_0 = initial tube radius
 ΔR = scale of the perturbed tube radius
 $\varepsilon = \Delta R/R$
 ω = angular frequency
 ρ = density of the fluid
 K = bulk modulus of the tube wall
 K_0 = unperturbed bulk modulus of the tube wall
 E = elasticity of the tube wall
 E_0 = unperturbed elasticity of the tube wall
 c_0 = velocity of the fluid
 Q = flux
 Q_0 = scale of the flux
 A = cross-section of the tube
 A_0 = unperturbed cross-section of the tube
 L_0 = longitudinal scale
 σ = Poisson's ratio
 ν = kinematic viscosity
 η = viscosity of the material
 ε_p = coefficient of the nonlinear stress strain characteristics

References

- [1] Nichols, W. W., and O'Rourke, M. F., 2005, *McDonald's Blood Flow in Arteries: Theoretical, Experimental and Clinical Principles*, 5th edition, Hodder Arnold, London.
- [2] Mitchell, G. F., Parise, H., Benjamin, E. J., Larson, M. G., Keyes, M. J., Vita, J. A., Vasan, R. S., and Levy, D., 2004, "Changes in Arterial Stiffness and Wave Reflection With Advancing Age in Healthy Men and Women," *Hypertension*, **43**, pp. 1239–1245.
- [3] Saito, M., Yamamoto, Y., Matsukawa, M., Watanabe, Y., Furuya, M., and Asada, T., 2009, "Simple Analysis of the Pulse Wave for Blood Vessel Evaluation," *Jpn. J. Appl. Phys.*, **48**, pp. 1–4.
- [4] Hope, S. A., Tay, D. B., Meredith, I. T., and Cameron, J. D., 2005, "Waveform Dispersion, Not Reflection, May Be the Major Determinant of Aortic Pressure Wave Morphology," *Am. J. Physiol.*, **289**, pp. H2497–H2502.
- [5] Murgo, J. P., Westerhof, N., Giolma, J. P., and Altobelli, S. A., 1980, "Aortic Input Impedance in Normal Man—Relationship to Pressure Wave Forms," *Circulation*, **62**, pp. 105–116.
- [6] Murgo, J. P., Westerhof, N., Giolma, J. P., and Altobelli, S. A., 1981, "Manipulation of Ascending Aortic Pressure and Flow Wave Reflections With the Valsalva Maneuver: Relationship to Input Impedance," *Circulation*, **63**, pp. 122–132.
- [7] Latham, R. D., Westerhof, N., Sipkema, P., Rubal, B. J., Reuderink, P., and Murgo, J. P., 1985, "Regional Wave Travel and Reflections Along the Human Aorta—A Study With Six Simultaneous Micromanometric Pressures," *Circulation*, **72**, pp. 1257–1269.
- [8] Hofmann, W., and Balászházy, I., 1991, "Particle Deposition Patterns Within Airway Bifurcations—Solution of the 3D Navier-Stokes Equation," *Radiat. Prot. Dosim.*, **38**, pp. 57–63.
- [9] Perktold, K., and Rappitsch, G., 1995, "Computer Simulation of Local Blood Flow and Vessel Mechanics in a Compliant Carotid Artery Bifurcation Model," *J. Biomech.*, **28**, pp. 845–856.
- [10] Theodorakakos, A., Gavaises, M., Andriotis, A., Zifan, A., Liatsis, P., Pantos, I., Efstathopoulos, E. P., and Katritsis, D., 2008, "Simulation of Cardiac Motion on Non-Newtonian, Pulsating Flow Development in the Human Left Anterior Descending Coronary Artery," *Phys. Med. Biol.*, **53**, pp. 4875–4892.
- [11] Dong, S., Insley, J., Karonis, N. T., Papka, M. E., Binns, J., and Karniadakis, G., 2006, "Simulating and Visualizing the Human Arterial System on the TeraGrid," *Future Gener. Comput. Syst.*, **22**, pp. 1011–1017.
- [12] Isaksen, J. G., Bazilevs, Y., Kvamsdal, T., Zhang, Y., Kaspersen, J. H., Waterloo, K., Romner, B., and Ingebrigtsen, T., 2008, "Determination of Wall Tension in Cerebral Artery Aneurysms by Numerical Simulation," *Stroke*, **39**, pp. 3172–3178.
- [13] Lagrée, P.-Y., 2000, "An Inverse Technique to Deduce the Elasticity of a Large Artery," *Eur. Phys. J. Appl. Phys.*, **9**, pp. 153–163.
- [14] Fullana, J., and Zaleski, S., 1999, "A Branched One-Dimensional Model of Vessel Networks," *J. Fluid Mech.*, **621**, pp. 183–204.
- [15] Zagzoule, M., and Marc-Vergnes, J., 1986, "A Global Mathematical Model of the Cerebral Circulation in Man," *J. Biomech.*, **19**(12), pp. 1015–1022.
- [16] Olufsen, M. S., Peskin, C. S., Kim, W. Y., Pedersen, E. M., Nadim, A., and Larsen, J., 2000, "Numerical Simulation and Experimental Validation of Blood Flow in Arteries With Structured-Tree Outflow Conditions," *Ann. Biomed. Eng.*, **28**, pp. 1281–1299.
- [17] Marchandise, E., Willemet, M., and Lacroix, V., 2009, "A Numerical Hemodynamic Tool for Predictive Vascular Surgery," *Med. Eng. Phys.*, **31**, pp. 131–144.
- [18] van de Vosse, F., and Stergiopoulos, N., 2011, "Pulse Wave Propagation in the Arterial Tree," *Annu. Rev. Fluid Mech.*, **43**, pp. 467–499.
- [19] Pedley, T. J., 1980, *The Fluid Mechanics of Large Blood Vessels*, Cambridge University Press, Cambridge, U.K.
- [20] Bessems, D., Rutten, M., and van de Vosse, F., 2001, "A Wave Propagation Model of Blood Flow in Large Vessels Using an Approximate Velocity Profile Function," *J. Fluid Mech.*, **580**, pp. 145–168.
- [21] Willemet, M., Lacroix, V., and Marchandise, E., 2011, "Inlet Boundary Conditions for Blood Flow Simulations in Truncated Arterial Networks," *J. Biomech.*, **44**, pp. 897–903.
- [22] Xiu, D., and Sherwin, S. J., 2007, "Parametric Uncertainty Analysis of Pulse Wave Propagation in a Model of a Human Arterial Network," *J. Comput. Phys.*, **226**, pp. 1385–1407.
- [23] Cohen, I. M., Kundu, P. K., and Hu, H. H., 2004, *Fluid Mechanics*, 3rd edition, Elsevier, New York.
- [24] van de Vosse, F., and van Dongen, M. E. H., 1998, "Cardiovascular Fluid Mechanics—Lecture Notes," Faculty of Applied Physics, Faculty of Mechanical Engineering, Eindhoven University of Technology, Eindhoven, Netherlands.
- [25] Westerhof, N., Bosman, F., De Vries, C. J., and Noordergraaf, A., 1969, "Analog Studies of the Human Systemic Arterial Tree," *J. Biomech.*, **2**, pp. 121–143.
- [26] Lorthois, S., Lagrée, P.-Y., Marc-Vergnes, J.-P., and Cassot, F., 2000, "Maximal Wall Shear Stress in Arterial Stenoses: Application to the Internal Carotid Arteries," *J. Biomech. Eng.*, **122**(6), pp. 661–666.
- [27] Vignon-Clementel, I. E., Figueroa, C. A., Jansen, K. E., and Taylor, C. A., 2010, "Outflow Boundary Conditions for 3D Simulations of Non-periodic Blood Flow and Pressure Fields in Deformable Arteries," *Comput. Meth. Biomech. Biomed. Eng.*, **13**(5), pp. 625–640.
- [28] Quarteroni, A., Ragni, S., and Veneziani, A., 2001, "Coupling Between Lumped and Distributed Models for Blood Flow Problems," *Comput. Visualization Sci.*, **4**(2), pp. 111–124.